This article has been accepted for inclusion in a future issue of this journal. Content is final as presented, with the exception of pagination.

A Novel State Transformation Approach to Tracking of Piecewise Linear Trajectories

Ali Bazaei, *Member, IEEE*, Zhiyong Chen, *Senior Member, IEEE*, Yuen Kuan Yong, *Member, IEEE*, and S. O. Reza Moheimani, *Fellow, IEEE*

***Abstract*— In this paper, we propose a novel approach for tracking of piecewise linear trajectories, such as triangular and staircase waveforms. We derive state and input transformations, which result in closed-loop error dynamics driven by a series of impulses. The proposed control structure takes the form of an output-feedback-feedforward system that is straightforward to implement. In contrast to the recently proposed tracking control methods for such trajectories, the closed-loop stability is not affected by the frequency of the desired triangular reference. The method is implemented on a nanopositioner serving as the scanning stage of an atomic force microscope.**

***Index Terms*— Feedback–feedforward, impulsive state multiplication (ISM), input and state transformations (ISTs), triangular references.**

I. Introduction

TRACKING of piecewise linear reference signals is a requirement in many applications. An example is the triangular waveform which is usually used as the desired reference signal for the fast lateral axis in raster scanning applications, such as scanning tunneling microscope and atomic force microscope (AFM) [1], [2], optical scanners [3], selective laser sintering systems [4], and in probe-based data storage devices [5]. In addition, any desired trajectory with arbitrary profile can accurately be approximated by a piecewise linear one.

In [6], tracking of triangular references was demonstrated by a signal transformation approach (STA), where signal transformation mappings were included at the plant input and output. Assuming a unity dc gain for the plant in STA, the mappings are designed to convert a ramp reference signal to the triangular reference and *vice versa*. Then, a feedback controller incorporating a double integrator was designed in [6] to have the plant with the transformation mappings track the ramp reference, while the plant output follows the triangular reference. A key benefit of STA is that the closed-loop bandwidth with the double integral controller can be very small compared with the bandwidth of an ordinary feedback system with a comparable tracking performance. The low closed-loop bandwidth is important in many applications, such as nanopositioning systems, where the amount of measurement noise affecting the plant through the feedback system can limit the positioning accuracy.

A drawback of STA is that the transient performance or even the stability of closed-loop systems is deteriorated as the frequency of the triangular reference increases [7]. This issue has not been resolved in the more advanced versions of STA, such as impulsive state multiplication (ISM), initialized-STA, and STA for arbitrary references [8]–[14]. We can confirm this deficiency by considering the stability criteria of STA and ISM, such as [7, Corollary 3] and [15, eq. (6)]. These criteria put limitations on the maximum magnitude of eigenvalues or norm of matrix exponential terms, whose arguments are the product of the stable closed-loop system matrix A and the half period T of the triangular reference. As a result, the stability criterion may not be satisfied as the frequency of the reference increases. This dependence of stability condition on the reference signal is mainly due to the switching actions or signals in ISM or STA that suddenly change the feedback loop in every half period of the triangular reference. As the reference frequency increases, the loop switching happens more frequently, deteriorating the stability of the hybrid system in the long run. Another important factor that can produce undesirable control performance or even instability in STA and ISM hybrid systems, while the closed-loop system matrix is stable, is the existence of dominant zeros in the plant or controller [7, Sec. 5.1].

In this paper, we propose a novel controller design method for tracking of piecewise linear references using input and state transformations (ISTs). The method allows a small control bandwidth to reduce the impact of measurement noise on the plant output while retaining closed-loop stability independent of the reference signal. We design ISTs such that the error dynamics are driven only by the second derivative of the reference, which consists of impulses at the breaking points of the reference profile. For a well-damped plant, the feedback control system comprises a double-integrator controller and a feedforward signal with no additional state estimation requirements. Compared with the STA and ISM methods, the feedback structure in IST method is much simpler and no signal transformation or switching block is incorporated within the loop. Hence, the transient performance and stability are not affected by the frequency of the reference signal.

Manuscript received June 17, 2016; revised November 10, 2016; accepted November 19, 2016. Manuscript received in final form January 9, 2017. This work was supported by Australian Research Council. Recommended by Associate Editor N. van de Wouw.

A. Bazaei, Z. Chen, and Y. K. Yong are with the School of Electrical and Computer Engineering, The University of Newcastle Australia, Callaghan, NSW 2308, Australia (e-mail: ali.bazaei@newcastle.edu.au; zhiyong.chen@newcastle.edu.au; yuenkuan.yong@newcastle.edu.au).

S. O. R. Moheimani is with the Department of Mechanical Engineering, Erik Jonsson School of Engineering and Computer Science, University of Texas at Dallas, Richardson, TX 75080 USA (e-mail: reza.moheimani@utdallas.edu).

Color versions of one or more of the figures in this paper are available online at http://ieeexplore.ieee.org.

Digital Object Identifier 10.1109/TCST.2017.2654061

1063-6536 © 2017 IEEE. Personal use is permitted, but republication/redistribution requires IEEE permission.
See http://www.ieee.org/publications_standards/publications/rights/index.html for more information.

This article has been accepted for inclusion in a future issue of this journal. Content is final as presented, with the exception of pagination.

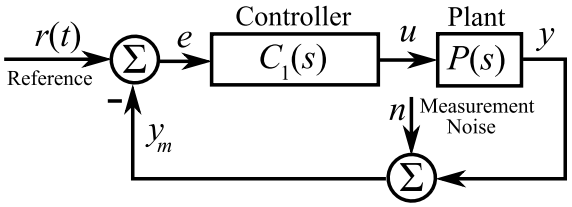

Fig. 1. 1-DoF feedback control system.

The corresponding control design procedure utilizes basic information about the plant, such as the nominal value of dc gain and dominant poles and zeros of the plant. In addition, the method relies on much less knowledge of the plant parameters and is simpler to design and implement compared with the contemporary feedback–feedforward control strategies [16], [17].

This paper is organized as follows. The control problem is described in Section II. In Section III, we derive ISTs that facilitate the solution to the control problem. The resulting transformations are used in Section IV to solve the control problem by the proposed IST method. In Appendix A, we show that the required parameters in the IST method are obtained by alternative expressions from a low frequency approximation of the plant transfer function. The simulations conducted in Section V illustrate the superiority of the IST method over the ISM and high-gain (HG) controllers in the presence of measurement noise. In Section VI, we experimentally implement the IST method on the lateral axes of a nanopositioner for tracking of triangular and continuous staircase reference signals. This section also addresses the adverse effect of cross coupling on the tracking error and a method to compensate for it. In Section VII, the IST controllers are used to scan a sample attached to the nanopositioner and obtain AFM images of the sample in constant-force-contact-mode. More details on the experimental setup have been provided in Appendix B.

II. Problem Statement

Consider a one-degree-of-freedom (1-DoF) feedback control system as shown in Fig. 1, where the closed-loop system is internally stable and provides zero steady-state tracking error to a constant reference signal. Such feedback system is identical to the ordinary feedback systems in the STA and ISM methods when signal transformation mappings are reduced to identity mappings in STA method or the state multiplication matrix and the feedforward gain are reduced to an identity matrix and zero in the ISM method, respectively [7], [15]. However, the desired reference signal is a piecewise linear waveform $r_{\rm pw}(t)$, which is assumed continuous and bounded. By *piecewise linear*, we mean that the time profile of the reference signal varies linearly with time during each time interval $t \in (T_{k-1}, T_k)$, as shown by the typical profile in Fig. 2. If the plant is open-loop stable with well-damped dominant poles, the integrator gains k_i and k_{ii} in the following double integral controller are easily obtained with adequate

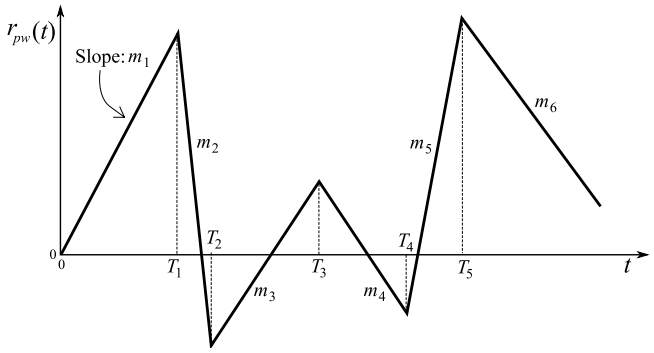

Fig. 2. Typical piecewise linear reference signal.

stability margins [7]:

$$C_1(s) = \frac{k_i s + k_{ii}}{s^2}. \tag{1}$$

In addition, the gains can be tuned to realize a desired low closed-loop bandwidth, while zero steady-state tracking error is guaranteed for a constant or ramp reference. However, tracking error of the 1-DoF feedback system with low bandwidth may not be acceptable for a piecewise linear reference. In the absence of noise and disturbances, the state dynamics in the 1-DoF system are only driven by the reference signal $r_{\rm pw}$, while the second time derivative of the reference signal is zero in almost all times except for impulses at specified time instants T_k, $k \in \{1, 2, 3, \ldots\}$. This is described as

$$\ddot{r}_{\rm pw} = \sum_{k=0}^{\infty} q_k \delta(t - T_k) \tag{2}$$

where $q_k = m_{k+1} - m_k$ is the abrupt change in the slope of the reference signal at $t = T_k$ and $m_0 = 0$. Hence, it is plausible to seek appropriate transformations through which the closed-loop dynamics of transformed states are possibly driven only by the second derivative of reference $r_{\rm pw}$, which is zero most of the time. The required transformations should also represent the tracking error as a linear combination of the transformed states, exclusively. More specifically, if $\overline{X}$ represents the transformed state vector of the closed-loop system, it would obey the following state dynamics:

$$\dot{\overline{X}} = A\overline{X} + E\ddot{r}_{\rm pw} \tag{3}$$

$$\overline{y} = C\overline{X} \tag{4}$$

where $\overline{y} = y - r_{\rm pw}$ is the tracking error, and A, E, and C are state-space matrices of the closed-loop system after the transformations are applied.

III. Synthesis of Transformations

Assume that the individual state-space representations of the nominal plant and controller in the 1-DoF system are as

$$\dot{X}_p = A_p X_p + B_p u \tag{5}$$

$$y = C_p X_p \tag{6}$$

This article has been accepted for inclusion in a future issue of this journal. Content is final as presented, with the exception of pagination.

and

$$\dot{X}_c = A_c X_c + B_c(r - y) \tag{7}$$
$$u = C_c X_c + D_c(r - y) \tag{8}$$

where measurement noise was not included for simplicity. The closed-loop dynamics of the 1-DoF feedback system can be stated as

$$\dot{X} = AX + Br \tag{9}$$
$$y = CX \tag{10}$$

where

$$X = \begin{bmatrix} X_p \\ X_c \end{bmatrix}; \quad A = \begin{bmatrix} A_p - B_p D_c C_p & B_p C_c \\ -B_c C_p & A_c \end{bmatrix} \tag{11}$$
$$B = \begin{bmatrix} B_p D_c \\ B_c \end{bmatrix}; \quad C = [C_p \quad \mathbf{0}]. \tag{12}$$

Before obtaining the desired closed-loop form in (3) and (4), we try to determine a transformed state-space representation of the plant in the form of

$$\dot{\overline{X}}_p = A_p \overline{X}_p + B_p \overline{u} + Q\ddot{r}_{\rm pw} \tag{13}$$
$$\overline{y} = C_p \overline{X}_p \tag{14}$$

where $\overline{u}$ is the transformed input of the plant to be determined and $\overline{X}_p$ is the transformed state of the plant. Because the second derivative of $r_{\rm pw}$ appears in the first time derivative of $\overline{X}_p$, one would intuitively choose the following expression for the transformed state of the plant:

$$\overline{X}_p = X_p + Rr_{\rm pw} + Q\dot{r}_{\rm pw} \tag{15}$$

where R and Q are constant vectors to be determined as well. Using (6) and (15), one can represent the error in the form of

$$r_{\rm pw} - y = (1 + C_p R)r_{\rm pw} + C_p Q\dot{r}_{\rm pw} - C_p \overline{X}_p. \tag{16}$$

Hence, (14) is satisfied if and only if the following conditions are satisfied:

$$C_p R = -1 \tag{17}$$
$$C_p Q = 0. \tag{18}$$

Denoting $g_o := P(0) = -C_p A_p^{-1} B_p$ as the plant dc gain, which is assumed nonzero, by inspection, we may choose the following expression for vector R to satisfy condition (17):

$$R = \frac{1}{g_o} A_p^{-1} B_p. \tag{19}$$

We also assume that the plant has no poles at the origin; hence, the inverse matrix is well defined. Taking the time derivative of (15) and using (5) and (19), we obtain the following condition to satisfy (13):

$$(R - A_p Q)\dot{r}_{\rm pw} = B_p\big(\overline{u} - u + g_o^{-1} r_{\rm pw}\big). \tag{20}$$

This condition is satisfied if and only if the constant vectors $R - A_p Q$ and B_p are parallel, implying

$$R - A_p Q = \lambda B_p \tag{21}$$

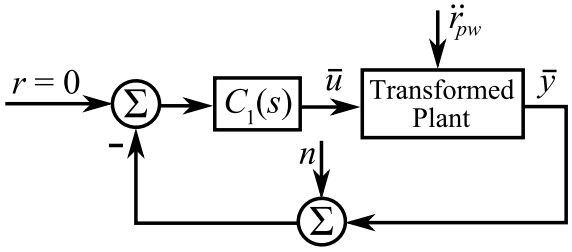

Fig. 3. 1-DoF feedback control system for the transformed plant.

where λ is a constant scalar to be determined. Using (18) and (21), we can simultaneously solve for λ and vector Q, obtaining

$$\lambda = -g_o^{-2} C_p A_p^{-2} B_p \tag{22}$$
$$Q = \big(g_o^{-1} A_p^{-1} - \lambda \mathrm{I}\big) A_p^{-1} B_p. \tag{23}$$

Having obtained vectors R and Q in terms of nominal plant parameters, the transformed state of the plant is completely determined from (15). Replacing (21) in (20) and equating the time-varying scalar coefficients of the constant vector B_p on both sides, we also obtain the input transformation as

$$\overline{u} = u - g_o^{-1} r_{\rm pw} + \lambda \dot{r}_{\rm pw}. \tag{24}$$

Lemma 1: Assume the reference signal $r_{\rm pw}(t)$ and a strictly proper plant described by (5) and (6) with no pole at the origin and a nonzero dc gain of g_o. Then, with the ISTs described by (15), (19), and (22)–(24) , the state-space representation of the open-loop plant satisfies (13). In addition, the output equation for the tracking error satisfies (14).

Proof: Having no poles at the origin ensures that matrix A_p is not singular and has an inverse. One can readily confirm the validity of (13) and (14) by following the foregoing synthesis procedure in a reverse direction. ■

IV. Proposed Controller

Comparing the transformed state equations of the plant in (13) and (14) with those of the plant in (5) and (6) reveals that a 1-DoF feedback system with the plant replaced by the transformed plant and $C_1(s)$ as the controller should have the same desired closed-loop system matrix A as in (11). A schematic of this 1-DoF feedback system is shown in Fig. 3, which is similar to the original feedback system except for the exogenous signal $\ddot{r}_{\rm pw}$. Since the output of the transformed plant is the tracking error, we reduce r to zero and replace y and u by $\overline{y}$ and $\overline{u}$, respectively, in (7) and (8) to obtain the following controller dynamics:

$$\dot{X}_c = A_c X_c + B_c(r_{\rm pw} - y) \tag{25}$$
$$\overline{u} = C_c X_c + D_c(r_{\rm pw} - y). \tag{26}$$

Now, the closed-loop system dynamics satisfy the desired state-space equations (3) and (4), where

$$\overline{X} = \begin{bmatrix} \overline{X}_p \\ X_c \end{bmatrix}, \quad E = \begin{bmatrix} Q \\ \mathbf{0} \end{bmatrix} \tag{27}$$

This article has been accepted for inclusion in a future issue of this journal. Content is final as presented, with the exception of pagination.

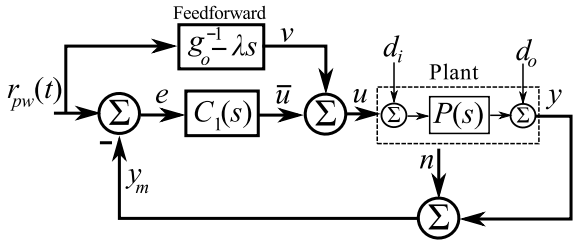

Fig. 4. Proposed control system applied to the original plant. The exogenous signals $d_i(t)$ and $d_o(t)$ represent the input and output disturbances applied to the plant, respectively.

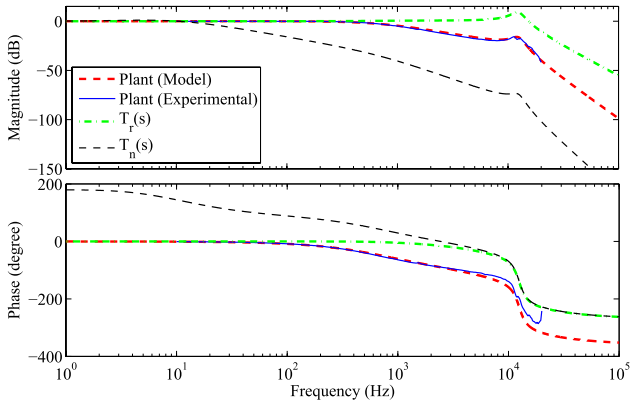

Fig. 5. Bode plots of the plant model in the illustrative example. The model well matches the experimental data within a 3-dB bandwidth of 720 Hz. Also included are Bode plots of the closed-loop transfer functions of the IST control system. The transfer function from the measurement noise has a 3-dB bandwidth of 19.44 Hz, whilst that of the reference signal is around 8 kHz.

and A and C are as defined in (11) and (12). Using (24), the plant manipulated input is obtained as

$$u = \overline{u} + v \tag{28}$$

where $v(t) = g_o^{-1} r_{\rm pw} - \lambda \dot{r}_{\rm pw}$ is a feedforward signal, and $\overline{u}$ is obtained from the feedback controller, according to (25) and (26). The proposed control system with respect to the original plant has an output-feedback–feedforward configuration as shown in Fig. 4.

Remark 2: Although the proposed method is based on a state transformation, the final controller does not require state measurement or estimation except for the plant output. Furthermore, the internal stability of the feedback system is not affected by the reference signal $r_{\rm pw}$. Moreover, to construct the feedforward signal requires knowledge of only two scalar parameters, i.e., the nonzero plant dc gain g_o and λ. These two plant parameters can be obtained from a low frequency approximation of plant transfer function without requiring exact knowledge of state-space matrices of the plant (see Appendix A).

V. Illustrative Example

Consider a stable unity dc gain plant ($g_o = 1$) whose frequency response is shown in Fig. 5. It is a model of an analog feedback control system, where the original plant is the x-axis of a lightly damped nanopositioner damped by

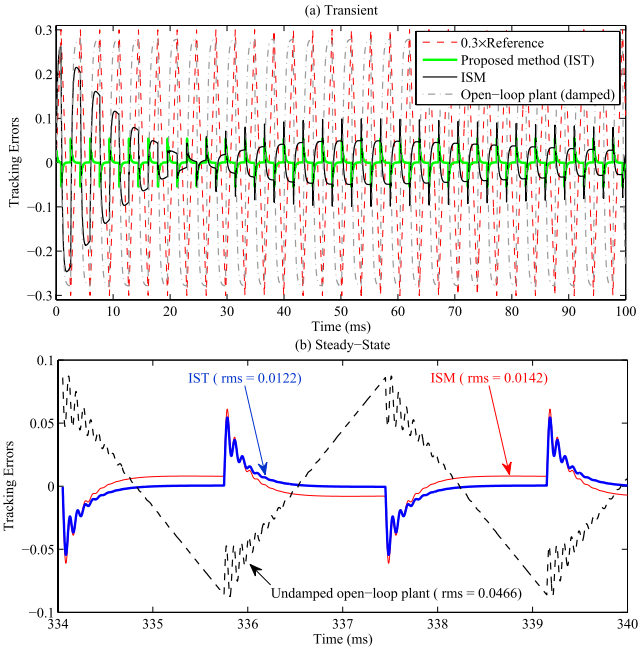

Fig. 6. (a) Scaled reference signal and tracking errors obtained by simulation in the absence of measurement noise. (b) Tracking errors at steady state.

an Integral-Resonant-Controller (IRC) and controlled by an integrator controller to have a unity dc gain, as detailed in Appendix B-A. A fourth-order LTI approximation of the plant can be represented as

$$P(s) = \frac{1}{\left(1-\frac{s}{p_1}\right)\left(1-\frac{s}{p_2}\right)\left(1+\frac{2\zeta s}{\omega_o}+\frac{s^2}{\omega_o^2}\right)} \tag{29}$$

where $p_1 = -4587$, $p_2 = -62830$, $\zeta = 0.12$, and $\omega_o = 78540$ rad/s. The objective is to track a triangular reference with the fundamental frequency of 300 Hz, which is 42% of the plant bandwidth while keeping the closed-loop bandwidth less than 20 Hz to limit the projected noise at the plant output y in Fig. 1. This is a challenging problem as in STA and ISM methods, the frequency of the triangular reference is usually selected less than 13% of the plant bandwidth for acceptable tracking and transient performances [15]. We can tune the coefficients of the double integral controller (1) as $k_i = 100$, and $k_{ii} = 2000$ to obtain a closed-loop system with stability margins 54.53 dB and 77.5° and a bandwidth of 19.44 Hz. To apply the proposed IST control method shown in Fig. 4, we obtained $\lambda \cong -2.37 \times 10^{-4}$ from (37). Also shown in Fig. 5 are the resulting frequency responses of the closed-loop transfer functions of the IST system from the reference signal $r_{\rm pw}$ and the noise source n to the plant output y, denoted by $T_r(s)$ and $T_n(s)$, respectively. Clearly, the feedforward term has considerably improved the bandwidth of $T_r(s)$ without affecting the small bandwidth of $T_n(s)$.

The resulting tracking error along with the triangular reference is shown in Fig. 6(a). We have also included in Fig. 6(a) the tracking errors of the same reference signal obtained by the ISM method using the same controller $C_1(s)$, as detailed in Fig. 7. Also included in Fig. 6(a), is the tracking error

This article has been accepted for inclusion in a future issue of this journal. Content is final as presented, with the exception of pagination.

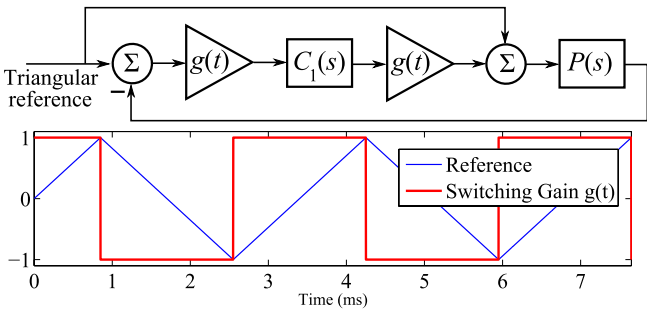

Fig. 7. Details of the ISM method for tracking of a triangular reference [9].

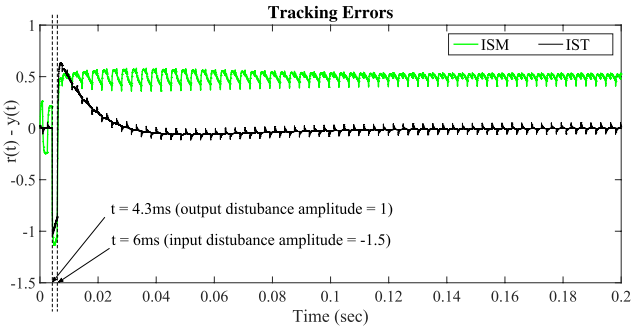

Fig. 8. Effect of application of constant output and input disturbances to the plant on the tracking performances of the IST and ISM methods.

resulting from a direct application of the reference to the unity dc gain open-loop plant. Clearly, the proposed IST method achieves a considerable improvement in the transient tracking performance compared with the other methods while keeping a low closed-loop bandwidth for the projected noise. For ISM and IST methods, Fig. 6(b) shows the profiles of the tracking errors and their root-mean-square (rms) values in steady state, where IST presents a better performance. Also included in Fig. 6(b) is the open-loop tracking error of the lightly damped nanopositioner described in Appendix B-A, where a constant gain was used to provide a unity dc gain and the triangular reference was directly applied to the undamped system.

Remark 3: In practice, such open-loop test is not desirable as the dc gain of the undamped plant is not a constant and varies with the amplitude of the excitation due to piezoelectric hysteresis and creep. Also, the displacement output is prone to slowly varying offset due to sensor drift.

Remark 4: Since the controller contains a double integrator, the proposed IST approach can reject constant and ramp disturbances. However, the ISM method cannot provide any disturbance rejection, as shown by the simulation results in Fig. 8. The transient time interval in the IST method during disturbance rejection is closely related to the small closed-loop bandwidth of the noise transfer function shown in Fig. 5. This transient time can be reduced by increasing the gains of the double integral controller, but at the expense of sacrificing the noise rejection performance. A key factor in improved performance of the IST method over ISM is the additional feedforward term of $-\lambda \dot{r}_{\mathrm{pw}}$. This factor is a piecewise constant term, which exerts abrupt changes to the plant through the feedforward path at the moments the rate of the reference signal changes, discontinuously. In the ISM method, where the feedforward term is only the continuous term of $g_o^{-1} r_{\mathrm{pw}}(t)$, the feedback controller undertakes discontinuities to exert abrupt changes on the plant and improve the tracking performance. However, such abrupt discontinuities in the feedback system can create poor transient (or even instability), as demonstrated in Fig. 6(a). On the other hand, in the IST method, the burden of providing discontinuities in the actuation signal has been transferred into the feedforward path.

Fig. 9 shows the simulation results of the IST control method with a high power measurement noise source. Clearly, the IST method can considerably attenuate the effect of measurement noise at the plant output and input without compromising the tracking performance.

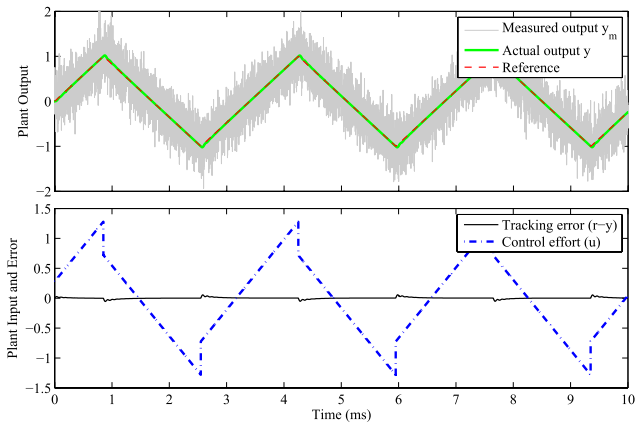

Fig. 9. Simulation results of the IST method in the presence of measurement noise.

For comparison purposes, we also designed an HG controller for the feedback system in Fig. 1. To do this, we used the mixed-sensitivity synthesis method that minimizes the H_∞ norm of the following cost function:

$$\left\| \begin{matrix} W_1(s)S_o(s) \\ W_2(s)R_o(s) \\ W_3(s)T_o(s) \end{matrix} \right\|_\infty \tag{30}$$

where $S_o(s) = (1/(1+C_1(s)P(s)))$, $R_o(s) = (C_1(s)/(1+C_1(s)P(s)))$, and $T_o(s) = (C_1(s)P(s)/(1+C_1(s)P(s)))$ refer to sensitivity, control sensitivity, and complementary sensitivity functions, respectively. Having selected the weight functions as

$$W_1(s) = \frac{s+201100}{2s+201.1}, \quad W_2 = 5, \quad W_3 = \frac{s+50270}{0.001s+100500} \tag{31}$$

the H_∞ optimization algorithm yields a sixth-order controller. After performing model reduction, we obtained the following HG controller:

$$C_1(s) = \frac{2.5\times 10^8 (s+4600)}{s(s+1.01\times 10^8)}. \tag{32}$$

The HG controller provides a closed-loop bandwidth of 2400 Hz (more than three times of the plant bandwidth) and stability margins of 9 dB and 77.6°. The magnitudes of the frequency responses of the weighting functions, controller, and

This article has been accepted for inclusion in a future issue of this journal. Content is final as presented, with the exception of pagination.

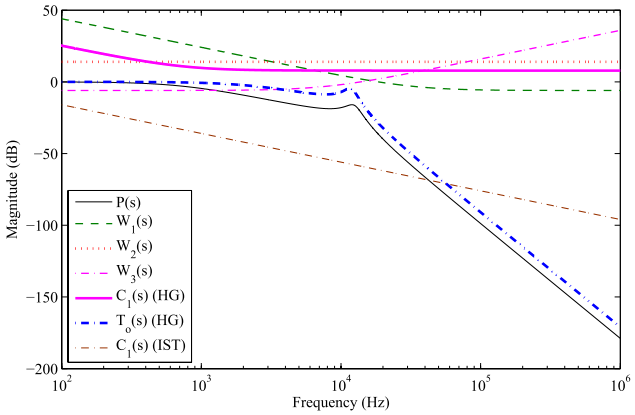

Fig. 10. Bode magnitude diagrams of the plant, weighting functions, HG controller, and the closed-loop transfer function $T_o(s)$ with HG controller. The magnitude of the double integral controller used in the IST method is also included for comparison.

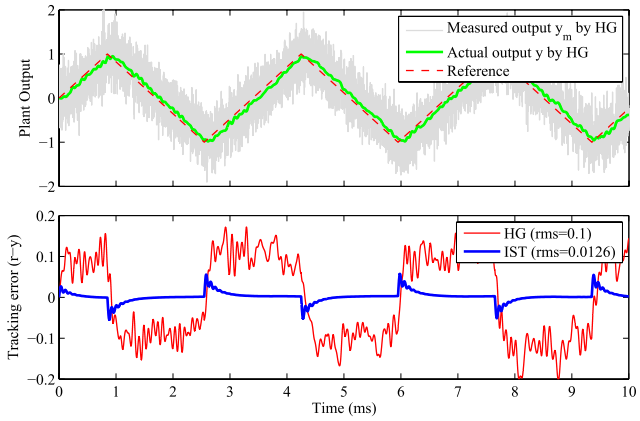

Fig. 11. Simulation results of the HG control system in the presence of measurement noise. The rms values of the tracking errors for both the HG and IST methods are also included.

the complementary sensitivity function are shown in Fig. 10. Fig. 11 shows the tracking performance of the HG controller in the presence of measurement noise and the same triangular reference as mentioned earlier, where the tracking error by the IST method is also included for comparison. Clearly, the IST method tracks the reference more accurately and the actual plant output is almost free from noise fluctuations.

VI. Experimental Results

In this section, we present the results of implementing IST controllers on the x- axis and the y-axis of a two-input-two-output plant described in Appendix B. The plant is a diagonally dominant system and has a unity dc gain for each axis as shown by the experimental frequency response in Fig. 5. The first IST controller is applied to the x-axis to track a triangular reference. The double-integrator controller and reference signal for the x-axis are as described in Section V, which are discretized at a sampling rate of 80 kHz for digital implementation in dSPACE. The parameter λ was gradually adjusted to -1.09×10^{-4} without affecting the stability, as shown in Fig. 4. The resulting tracking performance and plant

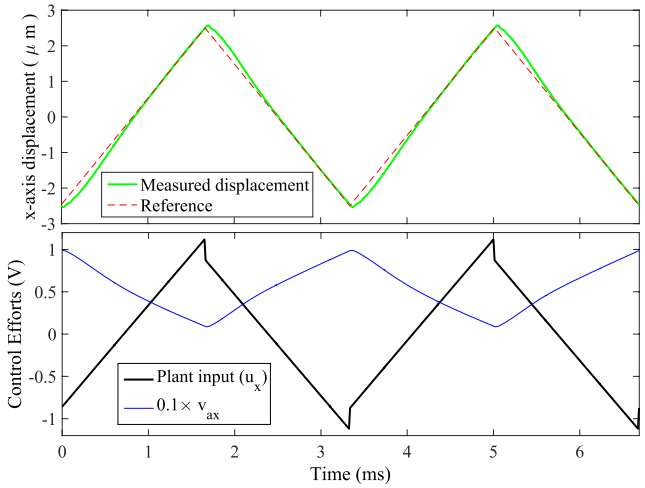

Fig. 12. Experimental results of the IST control method for the x-axis.

input are shown in Fig. 12, where a subscript x has been used for the variables to indicate they belong to the x-axis. Similarly, subscripts y and z refer to variables associated with the y-axis and the z-axis, respectively.

Remark 5: The experimental frequency response in Fig. 5 has been obtained by a small signal excitation. During a large signal operation, nonlinearities, such as hysteresis and creep in piezoelectric actuators, can change the actual bandwidth of the plant. Note that these nonlinearities are ignored during the simulation in Section V. Hence, the experimentally tuned value of λ is different from the calculated value. This experimental tuning capability also alleviates the burden of accurate calculation of λ in the IST control method.

For the y-axis, the desired reference is a continuous staircase signal, which is a piecewise linear trajectory. Hence, we can also apply an IST control method for the y-axis. Since the responses of the open-loop plant along the x-axis and the y-axis are very similar, the selected IST parameter values for the y-axis are identical to those of the x-axis except for the reference and the feedforward signals. Fig. 13 shows the experimental tracking performance of the ITS method in control of the y-axis displacement for the continuous staircase reference signal. In this experiment, we applied no actuation to the x-axis to prevent exerting disturbances on the y-axis from the cross-coupling (CC) effects. The tracking error for the y-axis is considerably smaller than that of the x-axis in Fig. 12 (rms values of 3.5 and 142 nm for the y and x, respectively). This can be justified by the fact that the slope and amplitude of the triangular reference signal for the x-axis are considerably higher than the slope and amplitude of each step in the staircase reference for the y-axis.

A. Effect of Cross-Coupling

For raster scanning, the x-axis tracks a 300-Hz triangular trajectory, while the y-axis has to follow a much slower reference signal, as shown in Fig. 14. During raster scanning, it is required to drive both axes simultaneously to cover a desired rectangular area. There exist mechanical interactions between

This article has been accepted for inclusion in a future issue of this journal. Content is final as presented, with the exception of pagination.

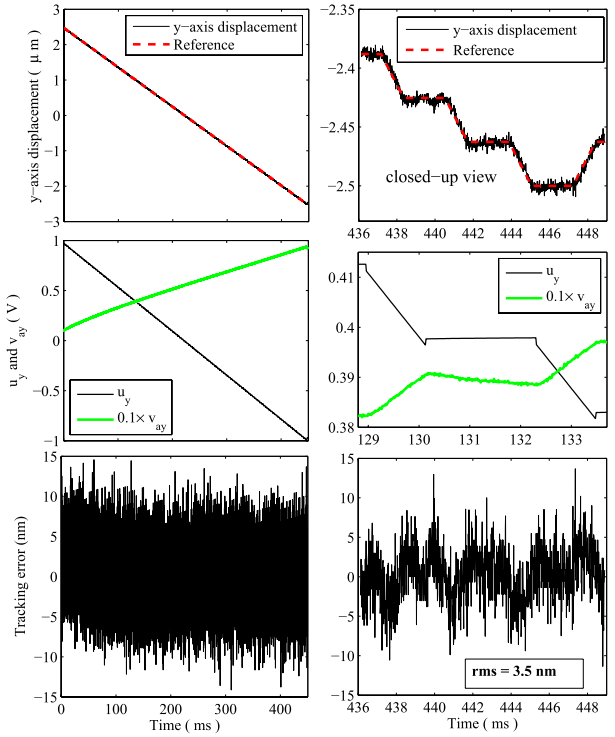

Fig. 13. Experimental results of the IST control method for the y-axis while the x-axis is not actuated.

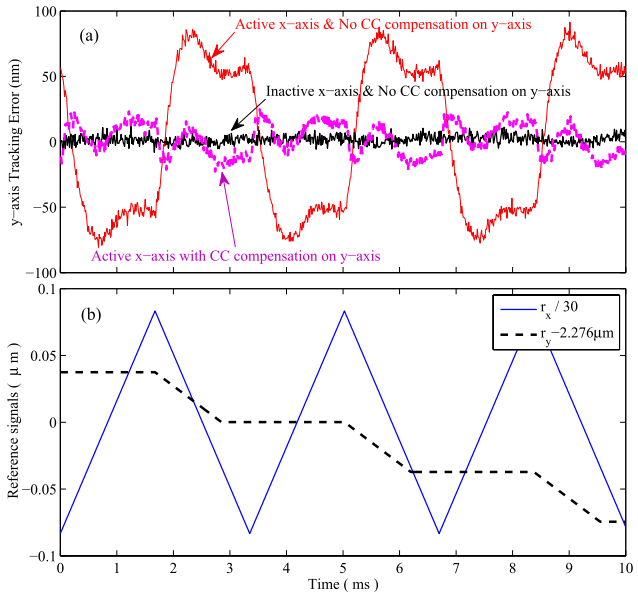

Fig. 14. (a) Effect of exciting the x-axis by the fast triangular reference on the tracking error of the slow axis (y-axis). (b) Triangular and staircase reference signals for the x and y axes denoted by r_x and r_y, respectively.

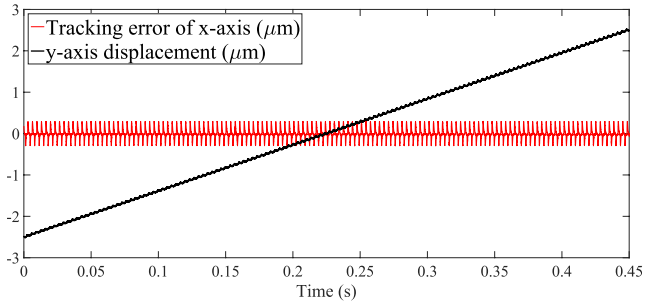

Fig. 15. Large displacement of the slow axis (y-axis) has almost not effect on the tracking error of the fast axis (x-axis), when the IST method is simultaneously applied to both axes for generating a raster scan trajectory.

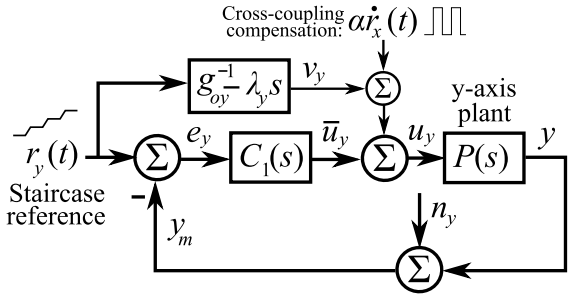

Fig. 16. Schematic of the IST control system for the y-axis with an additional feedforward signal from the x-axis for CC reduction.

the displacements along the x- and y-directions, known as CC. Although the level of CC in the nanopositioner is reasonably low [18], it has a noticeable effect on the tracking error of the y-axis (e_y), as shown in Fig. 14. Also included in Fig. 14 is the tracking error of the y-axis when the x-axis is not actuated. Note that the effect of y-axis excitation on the tracking error of the x-axis is insignificant, as shown in Fig. 15. The reason is that the y-axis tracks a slowly varying reference, and hence, its interaction on the x-axis is slowly varying too. This slowly varying disturbance on the x-axis can be easily canceled by the integral controllers included in the feedback system. The disturbance on the y-axis mainly originates from the x-axis motion, which is a rapidly varying signal. However, the bandwidth of the control system is not large enough to effectively cancel the rapidly varying disturbance on the y-axis.

We apply an empirical approach to reduce the tracking error for the y-axis without affecting the control bandwidth and stability. Since the profile of the tracking error in Fig. 14 is similar to the response of plant to a square wave actuation signal, we augmented the IST control law (28) for the y-axis by an additional feedforward signal $\alpha\dot{r}_x$, as shown in Fig. 16. Here, r_x refers to the triangular signal applied to the x-axis and α is a constant to be tuned, empirically. With a value of $\alpha = -3.8 \times 10^{-5}$, the resulting tracking error of the y-axis is also included in Fig. 14, while the x-axis is excited to track the triangular reference. With this CC compensation method, the rms value of tracking error is reduced to 11.6 nm, which is five times smaller than the error rms value before the compensation is applied.

VII. AFM Application

The imaging performance of the nanopositioner with the proposed control method is evaluated in this section. The nanopositioner was placed under a Nanosurf Easy Scan2 AFM as shown in Fig. 17. The AFM images were captured in constant-force contact mode with an external high-bandwidth

This article has been accepted for inclusion in a future issue of this journal. Content is final as presented, with the exception of pagination.

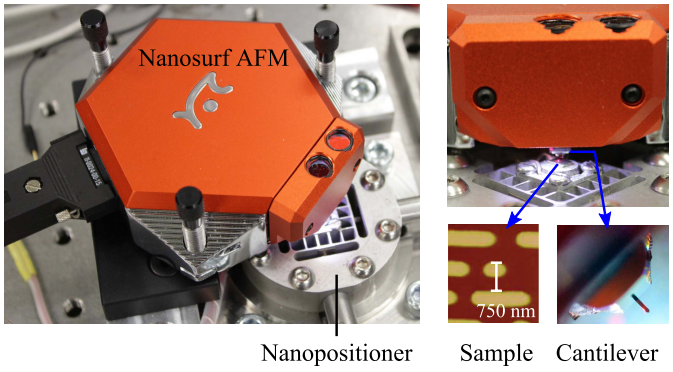

Fig. 17. Nanosurf AFM and the nanopositioner.

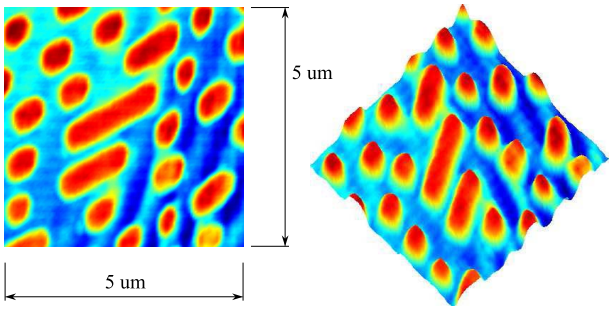

Fig. 18. 2-D and 3-D AFM images captured at 300-Hz raster line rate.

vertical feedback control loop as described in Appendix B. A 190-kHz cantilever from BudgetSensors (Tap190Al-G) which has a spring constant of 48 N/m was used to perform the scans. A calibration grating (750-HD) from Advanced Surface Microscopy, which has a nominal period of 750 nm and height of 100 nm, was used as a sample to evaluate the image performance of the system. Fig. 18 shows the resulting raster-scanned 2-D and 3-D images obtained at 300 Hz line rate from a 5 μm $\times$ 5 μm area of the sample. The image was obtained in about 0.45 s and is of high quality without artifacts caused by vibrations and insufficient tracking bandwidth. The image quality is further confirmed by comparison with the constant-force AFM image of the same sample as reported in [19], where the maximum lateral speed is reduced almost twice by an open-loop sinusoidal scan at 100 Hz.

VIII. Conclusion

For a 1-DoF stable output feedback control system, we derived IST mappings that impose a desirable closed-loop tracking performance with a piecewise constant reference signal. The resulting control system (IST) does not require state feedback but requires a feedforward signal, which is generated from the reference signal and its time derivative. Knowledge of low frequency approximation of the plant is enough to calculate the feedforward coefficients. These parameters can also be experimentally tuned without affecting the stability. In contrast to STA and ISM methods for tracking of triangular references, an increase in the reference frequency does not render the loop unstable in the IST method.

Simulation results reveal significant improvement of the tracking performance compared with that of the ISM method. In the presence of measurement noise, we also compared the performance of IST with that of an HG controller. In contrast to 120-fold increase of control bandwidth in the HG system, the rms value of the tracking error for the actual plant output in IST system is still eight times smaller than that of the HG system.

Effectiveness of the IST method was also examined on a custom-made 3-D nanopositioner for atomic force microscopy, where the IST method was also applied to the slow axis (y) to accurately follow a continuous staircase reference signal. Because of the small closed-loop bandwidth of the IST controllers, the y-axis suffers from a relatively large error induced by the CC from the fast axis (x). We were able to obtain a fivefold improvement in the y-axis error by including an additional feedforward signal for the y-axis proportional to the time derivative of the x-axis reference signal. This proportionality constant is empirically tuned without affecting the stability and bandwidth of the closed-loop system. We also demonstrated how the application of the proposed controllers on the nanopositioner can generate artifact free raster scan AFM images in a constant-force contact mode condition at a line rate of 300 Hz.

Appendix A
Feedforward Coefficients

In this section, we show that coefficients g_o and λ in the feedforward signal can be calculated from a low frequency approximation of the plant transfer function. Assume that the plant transfer function is as

$$P(s) = g_0 \frac{1 + \beta_1 s + \beta_2 s^2 + \cdots + \beta_{n-1} s^{n-1}}{1 + \alpha_1 s + \alpha_2 s^2 + \cdots + \alpha_n s^n}. \quad (33)$$

Since the plant has no poles at the origin $P(s)$ is differentiable at $s = 0$ and the first two terms of Taylor series expansion of (33) around the origin results in

$$P(s) = g_o + g_o(\beta_1 - \alpha_1)s + \sum_{k=2}^{\infty} \frac{1}{k!} \frac{d^k P(s)}{ds^k}\bigg|_{s=0} s^k. \quad (34)$$

An alternative way to represent the plant transfer function in terms of state-space matrices is as $P(s) = C_p(sI - A_p)^{-1}B_p$. Using this expression, the Taylor series expansion of $P(s)$ around $s = 0$ (specifically the first two terms) is as

$$P(s) = -C_p A_p^{-1} B_p - C_p A_p^{-2} B_p s - \sum_{k=2}^{\infty} C_p A_p^{-k-1} B_p s^k. \quad (35)$$

To obtain (35), the following Taylor expansion has been used around the origin:

$$(sI - A_p)^{-1} = -A_p^{-1}\left(I + A_p^{-1}s + \sum_{k=2}^{\infty} A_p^{-k} s^k\right). \quad (36)$$

Since the Taylor series coefficients of $P(s)$ are unique, the coefficients of s in the right-hand sides of (34) and (35) should be identical, i.e., $-C_p A_p^{-2} B_p = g_o(\beta_1 - \alpha_1)$. Using

This article has been accepted for inclusion in a future issue of this journal. Content is final as presented, with the exception of pagination.

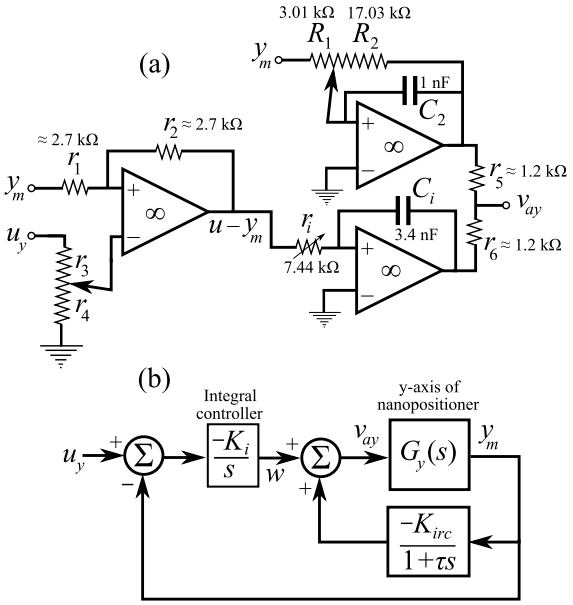

Fig. 19. (a) Circuit diagram of the analog controllers used for the y-axis of the nanopositioner. (b) Equivalent feedback system making a unity dc gain plant for the y-axis.

this equality and (22), we obtain an alternative expression for λ as

$$\lambda = g_o^{-1}(\beta_1 - \alpha_1). \tag{37}$$

Note that at sufficiently small frequencies, the numerator and denominator polynomials of the plant transfer function can be approximated by the first-order polynomials as

$$P(s) \approx g_o \frac{1+\beta_1 s}{1+\alpha_1 s}. \tag{38}$$

Hence, both g_o and λ can be approximated by the coefficients in (38), which is a low frequency approximation of the plant.

APPENDIX B
EXPERIMENTAL PLANT

This section describes the details of internal controllers that provide unity dc gain plants for each axis of the nanopositioner detailed in [18].

A. Lateral Axes

Fig. 19(a) shows the circuit diagram of the analog controller used for the y-axis, where v_{ay} is the output voltage applied to the piezodrive amplifier of the y-axis, y_m is the voltage from the capacitive sensor of the y-axis, and u is an auxiliary input (plant input in Fig. 1). Assuming ideal op-amps, a high input impedance for the piezodrive amplifier, and the following equalities:

$$\frac{r_1}{r_2} \cong \frac{r_3}{r_4}; \quad r_5 \cong r_6 \tag{39}$$

we can describe the feedback system as shown in Fig. 19(b), where

$$K_i = \frac{1}{2r_iC_i}; \quad K_{irc} = \frac{R_2}{2R_1}; \quad \tau = R_2C_2. \tag{40}$$

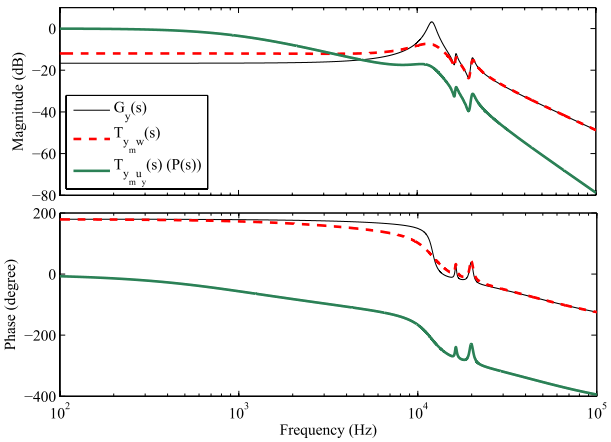

Fig. 20. Frequency responses of the open-loop y-axis ($G_y(s)$), damped system [transfer function from input w in Fig. 19 to output y_m ($T_{y_m w}$)], and the unity dc gain plant [$T_{y_m u_y}(s)$ or $P(s)$ for the y-axis].

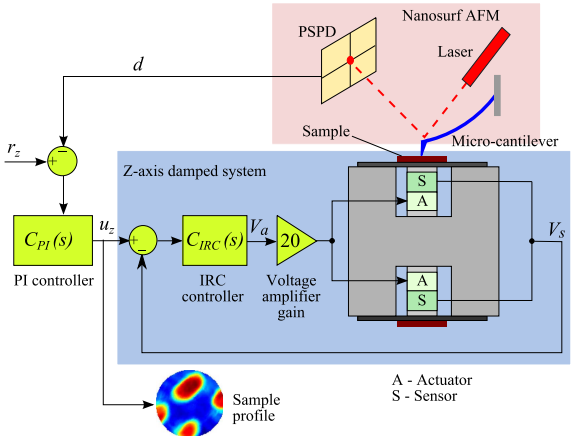

Fig. 21. Schematic of the z-axis control system.

The open-loop nanopositioner along the y-axis is a lightly damped system and has a negative dc gain as shown in Fig. 20. The low-pass-filter in the inner loop is used to damp the resonance and is equivalent to an Integral-Resonant-Controller (IRC) [20], [21]. The two resistors R_1 and R_2 were realized by a potentiometer to provide versatility of tuning the low-pass-filter coefficients, simultaneously. Having selected the element values reported in Fig. 19(a), the IRC controller reduces the dominant resonance peak at 12 kHz more than 16 dB as shown by the transfer function $T_{y_m w}$ of the inner loop in Fig. 20. To satisfy the first equality in (39), which is required for the subtraction block in Fig 19(b), r_3 and r_4 were realized by a potentiometer, as well. Another potentiometer was also used for r_i to tune the gain of the integrator. The integral controller provides a robust unity dc gain for the plant in Fig. 1 at the expense of a further reduction in the bandwidth, as shown by the transfer function of the plant ($P(s)$) in Fig. 20. The stability margins for the inner loop and the integral control loop are (6.9 dB, −82°) and (18.2 dB, 84°), respectively. The details of the unity dc gain plant for the x-axis are almost similar to those of the y-axis.

This article has been accepted for inclusion in a future issue of this journal. Content is final as presented, with the exception of pagination.

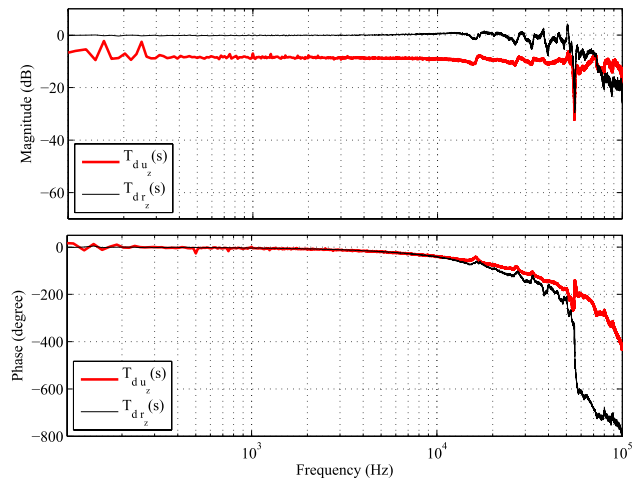

Fig. 22. Experimental frequency responses of the damped z-axis ($T_{du_z}(s)$) and the overall closed-loop system with the PI controller ($T_{dr_z}(s)$).

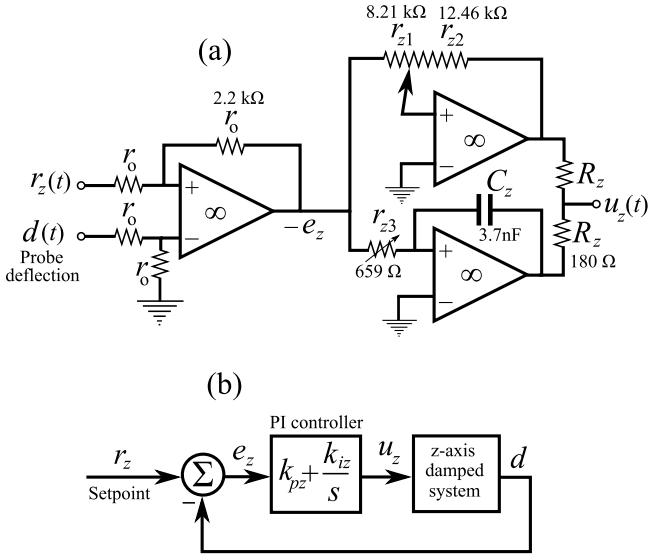

Fig. 23. (a) Circuit diagram of the analog PI controller for the z-axis. (b) Schematic of the equivalent PI control system.

B. Vertical Axis

The control system for the vertical axis aims to regulate the probe deflection in an atomic force microscope (AFM) at a constant setpoint to perform imaging in a constant force mode. The open-loop response of the nanopositioner along the z-axis has resonant modes at 20, 60, and 83 kHz. The resonant mode at 20 kHz is mechanically damped by a dual mounted structure and the remaining modes are damped by an IRC controller as shown in Fig. 21 [19]. The experimental frequency response of the damped z-axis from the auxiliary control input u_z to the probe deflection signal d ($T_{du_z}(s)$) is shown in Fig. 22. The schematic in Fig. 23 represents the analog PI controller used to regulate the probe deflection and the equivalent control system. Using the element values reported in Fig. 23(a), the proportional and integral gains are

$$k_{pz} = \frac{r_{z2}}{2r_{z1}} = 0.93 \tag{41}$$

$$k_{iz} = \frac{1}{2r_{z3}C_z} = 2.056 \times 10^5 \left(\frac{1}{\text{sec}}\right). \tag{42}$$

Resistances r_{z1}, r_{z2}, and r_{z3} were realized by potentiometers to readily adjust the proportional and integral gains to desired values. The PI controller provides stability margins 6.3 dB and 62°. The frequency response of the overall closed-loop control system for the z-axis is also included in Fig. 23, indicating a bandwidth around 50 kHz.

REFERENCES

[1] S. Devasia, E. Eleftheriou, and S. O. R. Moheimani, "A survey of control issues in nanopositioning," *IEEE Trans. Control Syst. Technol.*, vol. 15, no. 5, pp. 802–823, Sep. 2007.

[2] Y. K. Yong, S. O. R. Moheimani, B. J. Kenton, and K. K. Leang, "Invited review article: High-speed flexure-guided nanopositioning: Mechanical design and control issues," *Rev. Sci. Instrum.*, vol. 83, no. 12, p. 121101, Dec. 2012.

[3] J.-Y. Yen, Y.-C. Yeh, Y.-H. Peng, and J.-F. Lee, "Application of the continuous no-reset switching iterative learning control on a novel optical scanning system," *Mechatronics*, vol. 19, no. 1, pp. 65–75, Feb. 2009.

[4] D. Zhiqiang, Z. Zude, A. Wu, and C. Youping, "A linear drive system for the dynamic focus module of SLS machines," *Int. J. Adv. Manuf. Technol.*, vol. 32, nos. 11–12, pp. 1211–1217, May 2007.

[5] A. Pantazi *et al.*, "Probe-based ultrahigh-density storage technology," *IBM J. Res. Develop.*, vol. 52, nos. 4–5, pp. 493–511, Jul. 2008.

[6] A. Sebastian and S. O. R. Moheimani, "Signal transformation approach to fast nanopositioning," *Rev. Sci. Instrum.*, vol. 80, no. 7, p. 076101, Jul. 2009.

[7] A. Bazaei, S. O. R. Moheimani, and A. Sebastian, "An analysis of signal transformation approach to triangular waveform tracking," *Automatica*, vol. 47, no. 4, pp. 838–847, Apr. 2011.

[8] T. Tuma, A. Pantazi, J. Lygeros, and A. Sebastian, "Tracking of high frequency piecewise affine signals using impulsive control," in *Proc. 5th IFAC Symp. Mech. Syst.*, 2010, pp. 90–95.

[9] T. Tuma, A. Pantazi, J. Lygeros, and A. Sebastian, "Impulsive control for nanopositioning: Stability and performance," in *Proc. 14th Int. Conf. Hybrid Syst., Comput. Control*, Apr. 2011, pp. 173–180.

[10] T. Tuma, A. Sebastian, W. Häberle, J. Lygeros, and A. Pantazi, "Impulsive control for fast nanopositioning," *Nanotechnology*, vol. 22, no. 13, p. 135501, 2011.

[11] T. Tuma, A. Pantazi, J. Lygeros, and A. Sebastian, "Comparison of two non-linear control approaches to fast nanopositioning: Impulsive control and signal transformation," *Mechatronics*, vol. 22, no. 3, pp. 302–309, Apr. 2012.

[12] A. Bazaei and S. O. R. Moheimani, "Improving transient performance of signal transformation approach," in *Proc. IEEE Conf. Decision Control*, Maui, HI, USA, Dec. 2012, pp. 5059–5064.

[13] A. Bazaei and S. O. R. Moheimani, "Signal transformation approach to tracking control with arbitrary references," *IEEE Trans. Autom. Control*, vol. 57, no. 9, pp. 2294–2307, Sep. 2012.

[14] A. Bazaei, S. O. R. Moheimani, and Y. K. Yong, "Improvement of transient response in signal transformation approach by proper compensator initialization," *IEEE Trans. Control Syst. Technol.*, vol. 22, no. 2, pp. 729–736, Mar. 2014.

[15] T. Tuma, A. Pantazi, J. Lygeros, and A. Sebastian, "Nanopositioning with impulsive state multiplication: A hybrid control approach," *IEEE Trans. Control Syst. Technol.*, vol. 21, no. 4, pp. 1352–1364, Jul. 2013.

[16] K. K. Leang and S. Devasia, "Feedback-linearized inverse feedforward for creep, hysteresis, and vibration compensation in AFM piezoactuators," *IEEE Trans. Control Syst. Technol.*, vol. 15, no. 5, pp. 927–935, Sep. 2007.

[17] H. Habibullah, H. R. Pota, I. R. Petersen, and M. S. Rana, "Tracking of triangular reference signals using LQG controllers for lateral positioning of an AFM scanner stage," *IEEE/ASME Trans. Mechatronics*, vol. 19, no. 4, pp. 1105–1114, Aug. 2014.

This article has been accepted for inclusion in a future issue of this journal. Content is final as presented, with the exception of pagination.

[18] Y. K. Yong, B. Bhikkaji, and S. O. R. Moheimani, "Design, modeling, and FPAA-based control of a high-speed atomic force microscope nanopositioner," *IEEE/ASME Trans. Mechatronics*, vol. 18, no. 3, pp. 1060–1071, Jun. 2013, doi: 10.1109/TMECH.2012.2194161.
[19] Y. K. Yong and S. O. R. Moheimani, "Collocated Z-axis control of a high-speed nanopositioner for video-rate atomic force microscopy," *IEEE Trans. Nanotechnol.*, vol. 14, no. 2, pp. 338–345, Mar. 2015.
[20] S. S. Aphale, A. J. Fleming, and S. O. R. Moheimani, "Integral resonant control of collocated smart structures," *Smart Mater. Struct.*, vol. 16, no. 2, pp. 439–446, 2007.
[21] B. Bhikkaji and S. O. R. Moheimani, "Integral resonant control of a piezoelectric tube actuator for fast nanoscale positioning," *IEEE/ASME Trans. Mechatronics*, vol. 13, no. 5, pp. 530–537, Oct. 2008.

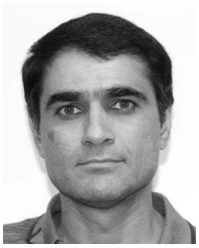

Ali Bazaei (M'10) received the B.Sc. and M.Sc. degrees in electrical engineering from Shiraz University, Shiraz, Iran, in 1992 and 1995, respectively, and the Ph.D. degrees from Tarbiat Modares University, Tehran, Iran, in 2004, and from the University of Western Ontario, London, ON, Canada, in, 2009.

From 1995 to 2000, he was an Instructor with Yazd University, Yazd, Iran. From 2004 to 2005, he was a Research Assistant with the Department of Electrical and Computer Engineering, University of Western Ontario. Since 2009, he held a post-doctoral research fellowship and research associate positions with the School of Electrical Engineering and Computer Science, The University of Newcastle Australia, Callaghan, NSW, Australia. He is the author of over 50 peer reviewed articles. His current research interests include the general area of nonlinear systems, including control and the modeling of structurally flexible systems, friction modeling and compensation, neural networks, and microposition sensors.

Zhiyong Chen (S'03–SM'13) received the B.E. degree from the University of Science and Technology of China, Hefei, China, in 2000, and the M.Phil. and Ph.D. degrees from The Chinese University of Hong Kong in 2002, and 2005, respectively.

He was a Research Associate with the University of Virginia, Charlottesville, VA, USA, from 2005 to 2006. He is currently an Associate Professor with The University of Newcastle Australia, Callaghan, NSW, Australia. His current research interests include nonlinear systems and control, nanopositioning systems, biological systems, and multiagent systems.

Dr. Chen is an Associate Editor of the IEEE TRANSACTIONS ON AUTOMATIC CONTROL and the IEEE TRANSACTIONS ON CYBERNETICS.

Yuen Kuan Yong (M'09) received the B.Eng. degree (Hons.) in mechatronic engineering and the Ph.D. degree in mechanical engineering from The University of Adelaide, Adelaide SA, Australia, in 2001 and 2007, respectively.

She is currently an Australian Research Council DECRA Fellow with the School of Electrical Engineering and Computer Science, The University of Newcastle Australia, Callaghan NSW, Australia. Her current research interests include the design and control of nanopositioning systems, high-speed atomic force microscopy, the finite-element analysis of smart materials and structures, sensing and actuation, and the design and control of miniature robots.

Dr. Yong is a recipient of the 2016 and 2008 IEEE/ASME International Conference on Advanced Intelligent Mechatronics Best Conference Paper Finalist Award, and the 2014 University of Newcastle Vice-Chancellor's Awards for Research Excellence. She is an Associate Editor of the *Frontiers in Mechanical Engineering* (specialty section Mechatronics) and the *International Journal of Advanced Robotic Systems*. She is also a Steering Committee Member for the International Conference on Manipulation, Automation, and Robotics at Small Scales.

S. O. Reza Moheimani (F'11) currently holds the James Von Ehr Distinguished Chair in science and technology with the Department of Mechanical Engineering, University of Texas at Dallas, Richardson, TX, USA. His current research interests include ultrahigh-precision mechatronic systems, with particular emphasis on dynamics and control at the nanometer scale, including the applications of control and estimation in nanopositioning systems for high-speed scanning probe microscopy and nanomanufacturing, the modeling, and control of microcantilever-based devices, the control of microactuators in microelectromechanical systems, and the design, modeling, and control of micromachined nanopositioners for on-chip scanningprobe microscopy.

Dr. Moheimani is a fellow of the IFAC and the Institute of Physics, U.K. He was a recipient of number of awards, including the IFAC Nathaniel B. Nichols Medal in 2014, the IFAC Mechatronic Systems Award in 2013, the IEEE Control Systems Technology Award in 2009, the IEEE TRANSACTIONS ON CONTROL SYSTEMS TECHNOLOGY OUTSTANDING PAPER AWARD in 2007, and several best paper awards in various conferences. He is currently the Chair of the IFAC Technical Committee on Mechatronic Systems. He is Editor-in-Chief of Mechatronics and has served on the Editorial Board of a number of other journals, including the IEEE TRANSACTIONS ON MECHATRONICS, the IEEE TRANSACTIONS ON CONTROL SYSTEMS TECHNOLOGY, and the *Control Engineering Practice*.